Dynamic least-squares kernel density modeling of Fokker-Planck equations with application to neural population

Babak Shotorban
Department of Mechanical and Aerospace Engineering, The University of Alabama in Huntsville, Huntsville, Alabama 35899, USA
(Received 1 December 2009; revised manuscript received 13 March 2010; published 30 April 2010)

The dynamic least-squares kernel density (LSQKD) model [C. Pantano and B. Shotorban, Phys. Rev. E **76**, 066705 (2007)] is used to solve the Fokker-Planck equations. In this model the probability density function (PDF) is approximated by a linear combination of basis functions with unknown parameters whose governing equations are determined by a global least-squares approximation of the PDF in the phase space. In this work basis functions are set to be Gaussian for which the mean, variance, and covariances are governed by a set of partial differential equations (PDEs) or ordinary differential equations (ODEs) depending on what phase-space variables are approximated by Gaussian functions. Three sample problems of univariate double-well potential, bivariate bistable neurodynamical system [G. Deco and D. Martí, Phys. Rev. E **75**, 031913 (2007)], and bivariate Brownian particles in a nonuniform gas are studied. The LSQKD is verified for these problems as its results are compared against the results of the method of characteristics in nondiffusive cases and the stochastic particle method in diffusive cases. For the double-well potential problem it is observed that for low to moderate diffusivity the dynamic LSQKD well predicts the stationary PDF for which there is an exact solution. A similar observation is made for the bistable neurodynamical system. In both these problems least-squares approximation is made on all phase-space variables resulting in a set of ODEs with time as the independent variable for the Gaussian function parameters. In the problem of Brownian particles in a nonuniform gas, this approximation is made only for the particle velocity variable leading to a set of PDEs with time and particle position as independent variables. Solving these PDEs, a very good performance by LSQKD is observed for a wide range of diffusivities.

DOI: 10.1103/PhysRevE.81.046706 PACS number(s): 05.10.−a, 87.15.A−

I. INTRODUCTION

Stochastic phenomena can be sometimes described by the Fokker-Planck equation

$$\frac{\partial p(\mathbf{x},t)}{\partial t} = -\sum_{i=1}^{N} \frac{\partial}{\partial x_i}[\mathcal{A}_i(\mathbf{x})p(\mathbf{x},t)] + \frac{1}{2}\sum_{i=1}^{N}\sum_{j=1}^{N} \frac{\partial^2}{\partial x_i \partial x_j}[\mathcal{B}_{ij}(\mathbf{x})p(\mathbf{x},t)], \quad (1)$$

where $p(\mathbf{x},t)$ is the probability density function (PDF) with t and $\mathbf{x}=(x_1,\ldots,x_N)$ representing time and the phase-space multivariate vector, respectively. Our aim in this work is to apply the dynamic least-squares kernel density (LSQKD) modeling [1] for approximating $p(\mathbf{x},t)$. In particular, we develop the LSQKD formulation for the PDFs with bimodal shapes that can be seen in various stochastic phenomena for which there are two stable states [2–6].

The dynamic LSQKD modeling is based on a global approximation of PDF in the phase space. The PDF is approximated through a linear combination of elementary functions such as Gaussian functions. Such approximations are known as kernel density estimation proposed and employed in [7–10] for the "static" problems in which there is no time involvement. In "dynamic" modeling, introduced for time-dependent PDFs governed by partial differential equations (PDEs), the parameters of elementary functions are assumed to be functions of time and some of the phase-space variables [1]. These parameters are governed by a set of differential equations which are determined by minimizing—in a least-squares sense—the residual resulting from the substitution of the approximate PDF in the partial differential equation governing the PDF. The non-negativity and normalization conditions of PDF are enforced at all times treating them as constraints of the minimization problem.

The dynamic LSQKD modeling was first employed for the study of evolution of uncertainties in the initial conditions of the Liouville equation [1]. In that work a system governed by a Riccati equation and a particle moving in a fluid under the influence of Stokes drag force were studied. The results exhibited reasonably good agreements when compared with the exact solution obtained for the original Liouville equation through the method of characteristics (MC).

The focus of the current study is on the dynamic LSQKD modeling of Fokker-Planck equations with specific attention to examples with bimodal PDFs. In Sec. II, we formulate the dynamic LSQKD for the Fokker-Planck equation. Three sample problems of double-well potential in the univariate case, bistable neurodynamical system [3], and Brownian particles in nonuniform gas solved through the model are presented in Sec. III. In Sec. IV the methodology employed in this work to verify the LSQKD for Fokker-Planck equations is illustrated. In Sec. V results obtained for sample problems are discussed and finally some conclusions are remarked in Sec. VI.

II. DYNAMIC LSQKD FOR FOKKER-PLANCK EQUATION

In the LSQKD modeling of the Fokker-Planck equation (1), $p(\mathbf{x},t)$ is approximated in the general form by

$$p(\mathbf{x},t) \approx \sum_{k=1}^{K} a_k(\mathbf{y},t) p_k(\mathbf{z},\mathbf{d}(\mathbf{y},t)), \tag{2}$$

where $\mathbf{y}=(y_1,\ldots,y_L)$ and $\mathbf{z}=(z_1,\ldots,z_{N-L})$ satisfying $\mathbf{y}\cup\mathbf{z}=\mathbf{x}$. In Eq. (2), p_k is a known function of $\mathbf{z}$ and $\mathbf{d}=(d_1,\ldots,d_M)$, whereas a_k and d_i are unknown functions of $\mathbf{y}$ and t. For a probabilistic system which exhibits a multimodal behavior for PDF, the approximation made in Eq. (2) for the form of PDF is of interest since with a number of modes of the PDF equal to K, each p_k in Eq. (2) corresponds to one mode weighted by a_k.

$p(\mathbf{x},t)$ approximated by Eq. (2) does not satisfy Eq. (1) and results in a residual. The least-squares method is used to minimize the residual. That is to minimize the functional

$$J = \int_{\Omega_y}\int_{\Omega_z} r^2 d\mathbf{z}d\mathbf{y} + \gamma(t)\left(1 - \int_{\Omega_y}\int_{\Omega_z} p d\mathbf{z}d\mathbf{y}\right), \tag{3}$$

where the last term is to account for the constraint of the normalization condition of the PDF by the Lagrange multiplier method. In the LSQKD formulation, we assume that p_k has such a property that

$$\int_{\Omega_z} p_k(\mathbf{z},\mathbf{d}) d\mathbf{z} = 1. \tag{4}$$

Applying the normalization condition of the PDF on this equation gives

$$\int_{\Omega_y} \sum_{k=1}^{K} a_k(\mathbf{y},t) d\mathbf{y} = 1. \tag{5}$$

It can be shown that this equality is satisfied at any t if it is satisfied at $t=0$ and

$$\int_{\Omega_y} \sum_{k=1}^{K} \dot{a}_k(\mathbf{y},t) d\mathbf{y} = 0, \tag{6}$$

where for any function $\dot{f}=\partial f/\partial t$. Thus, with Eq. (6) as the constraint, the functional J in Eq. (3) is simplified to

$$J = \int_{\Omega_y} \left[F + \gamma(t) \sum_{k=1}^{K} \dot{a}_k(\mathbf{y},t) \right] d\mathbf{y}, \tag{7}$$

where

$$F = \int_{\Omega_z} r^2 d\mathbf{z}. \tag{8}$$

The minimization is carried out by differentiation of J with respect to $\dot{a}_k$, $\dot{d}_m$, and γ in the dynamic LSQKD modeling. This minimization method has been introduced and employed for the dynamic LSQKD modeling of Liouville equation by [1] providing the general formulation which is applicable in the current work.

In order to clarify the LSQKD formulation for the Fokker-Planck equation, here we show how it is done for bivariate cases where $\mathbf{z}=\{x_1,x_2\}$ and $\mathbf{y}=\varnothing$, where $\varnothing$ is the empty set. We assume that the basis functions are $p_k=g_k$, where g_k denotes a bivariate Gaussian; Eq. (2) reads

$$p(x_1,x_2,t) = a_1(t)g_1(x_1,x_2,t) + a_2(t)g_2(x_1,x_2,t), \tag{9}$$

where

$$g_k(x_1,x_2,t) = \frac{1}{2\pi|\mathbf{\Sigma}_k|^{1/2}} \exp\left(-\frac{1}{2}\mathbf{y}_k^T \mathbf{\Sigma}_k^{-1} \mathbf{y}_k\right), \tag{10}$$

where

$$\mathbf{y}_k = \begin{pmatrix} x_1 - \mu_{1,k}(t) \\ x_2 - \mu_{2,k}(t) \end{pmatrix}, \tag{11}$$

$$\mathbf{\Sigma}_k = \begin{pmatrix} \sigma_{1,k}^2(t) & c_k(t) \\ c_k(t) & \sigma_{2,k}^2(t) \end{pmatrix}, \tag{12}$$

where $\mu_{i,k}(t)$, $\sigma_{i,k}^2(t)$, and $c_k(t)$ denote time varying means, variances, and cross covariances, respectively. $\mathbf{\Sigma}_k$ is the covariance matrix associated with g_k.

Approximating $p(x_1,x_2,t)$ by Eq. (9) and then substituting it in Eq. (1) results in the residual r given in the matrix form by

$$r = \mathbf{G}^T\dot{\mathbf{a}} + \dot{\mathbf{a}}^T\mathbf{M}\dot{\mathbf{b}} + \mathbf{a}^T\mathbf{Q}, \tag{13}$$

where $\dot{\mathbf{a}}=d\mathbf{a}/dt$ and $\dot{\mathbf{b}}=d\mathbf{b}/dt$ are, respectively, time derivatives of

$$\mathbf{a} = (a_1 \quad a_2)^T, \tag{14}$$

$$\mathbf{b} = (\mu_{1,1} \quad \mu_{2,1} \quad \sigma_{1,1} \quad \sigma_{2,1} \quad c_1 \quad \mu_{1,2} \quad \mu_{2,2} \quad \sigma_{1,2} \quad \sigma_{2,2} \quad c_2)^T. \tag{15}$$

Superscript T denotes the transpose operation. The rest of terms in Eq. (13) are defined as follows:

$$\mathbf{G} = (g_1 \quad g_2)^T, \tag{16}$$

$$\mathbf{M} = \frac{\partial \mathbf{G}}{\partial \mathbf{b}} = \begin{pmatrix} \frac{\partial g_1}{\partial \mu_{1,1}} & \frac{\partial g_1}{\partial \mu_{2,1}} & \frac{\partial g_1}{\partial \sigma_{1,1}} & \frac{\partial g_1}{\partial \sigma_{2,1}} & \frac{\partial g_1}{\partial c_1} & 0 & 0 & 0 & 0 & 0 \\ 0 & 0 & 0 & 0 & 0 & \frac{\partial g_2}{\partial \mu_{1,2}} & \frac{\partial g_2}{\partial \mu_{2,2}} & \frac{\partial g_2}{\partial \sigma_{1,2}} & \frac{\partial g_2}{\partial \sigma_{2,2}} & \frac{\partial g_2}{\partial c_2} \end{pmatrix}, \tag{17}$$

$$\mathbf{Q} = (Q(g_1) \quad Q(g_2))^T. \tag{18}$$

Vector components in Eq. (18) are calculated by

$$Q(g_k) = \sum_{i=1}^{2} \frac{\partial}{\partial x_i}[\mathcal{A}_i(\mathbf{x}) g_k(x_1, x_2, t)] - \sum_{i=1}^{2}\sum_{j=1}^{2} \frac{1}{2}\frac{\partial^2}{\partial x_i \partial x_j}[\mathcal{B}_{ij}(\mathbf{x}) g_k(x_1, x_2, t)], \tag{19}$$

which, in fact, accounts for all terms in Eq. (1) excluding the time derivative term on the left-hand side when p is substituted by g_k.

Integrating both sides of Eq. (9), the condition

$$a_1(t) + a_2(t) = 1 \tag{20}$$

must be satisfied at all times since the normalization condition of the probability density function, i.e., $\int\int p dx_1 x_2 = 1$ in Eq. (9), must be met noting that for the Gaussian function $\int\int g_k dx_1 x_2 = 1$. Provided that Eq. (20) is satisfied at the initial time, i.e., $a_1(0) + a_2(0) = 1$, Eq. (20) is equivalent to

$$\dot{a}_1 + \dot{a}_2 = 0. \tag{21}$$

According to the LSQKD modeling, the cost function [11] is constructed by

$$J = \int\int r^2 dx_1 x_2 + \gamma(t)(\dot{a}_1 + \dot{a}_2), \tag{22}$$

where $\gamma(t)$ is the Lagrangian multiplier that enforces the constraint given by Eq. (21). The derivatives of J with respect to components of $\dot{\mathbf{a}}$ and $\dot{\mathbf{b}}$, and $\gamma(t)$ are set to zero in order to minimize r in a least-squares sense. This results in the matrix-form equation

$$\begin{pmatrix} \mathbf{A} & \mathbf{C}^T & \mathbf{1} \\ \mathbf{C} & \mathbf{B} & \mathbf{0} \\ \mathbf{1}^T & \mathbf{0}^T & 0 \end{pmatrix} \begin{pmatrix} \dot{\mathbf{a}} \\ \dot{\mathbf{b}} \\ \gamma \end{pmatrix} = - \begin{pmatrix} \mathbf{D} \\ \mathbf{E} \\ 0 \end{pmatrix}, \tag{23}$$

where

$$\mathbf{A} = \int\int \mathbf{G}\mathbf{G}^T dx_1 x_2, \tag{24}$$

$$\mathbf{B} = \int\int \mathbf{M}^T \mathbf{a}\mathbf{a}^T \mathbf{M} dx_1 x_2, \tag{25}$$

$$\mathbf{C} = \int\int \mathbf{M}^T \mathbf{a}\mathbf{G}^T dx_1 x_2, \tag{26}$$

$$\mathbf{D} = \int\int \mathbf{a}^T \mathbf{Q}\mathbf{G} dx_1 x_2, \tag{27}$$

$$\mathbf{E} = \int\int \mathbf{a}^T \mathbf{Q}\mathbf{M}^T \mathbf{a} dx_1 x_2, \tag{28}$$

where $\mathbf{a}$, $\mathbf{G}$, and $\mathbf{M}$ are given by Eqs. (14), (16), and (17), respectively, and

$$\mathbf{Q} = (Q(g_1) \quad Q(g_2))^T. \tag{29}$$

In Eq. (23),

$$\mathbf{1} = (1 \quad 1)^T, \tag{30}$$

$$\mathbf{0} = (0 \quad 0 \quad 0 \quad 0 \quad 0 \quad 0 \quad 0 \quad 0 \quad 0 \quad 0)^T \tag{31}$$

are the unit and zero vectors, respectively. Elements in matrices seen Eqs. (24)–(28) can be calculated using a math scripting language. We use MATHEMATICA, a product of Wolfram Research, Inc., in this work.

III. SAMPLE PROBLEMS

To conduct the verification of the dynamic LSQKD modeling for the Fokker-Planck equations we focus on three sample problems of double-well potential, stochastic bistable neurodynamical system, and Brownian particles in a nonuniform gas.

A. Double-well potential problem

This problem may occur where the drift coefficient $\mathcal{A}(\mathbf{x})$ in Eq. (1) is the gradient of a potential function with two minima. Therefore, there are two stable states for the system. Such a problem has applications in a large number of electronic, chemical, and physical systems [2]. Here, we only consider a univariate case. So the Fokker-Planck equation (1) is simplified to

$$\frac{\partial p}{\partial t} = -\frac{\partial}{\partial x}[\mathcal{U}'(x)p] + \mathcal{D}\frac{\partial^2 p}{\partial x^2}, \tag{32}$$

where $\mathcal{U}(x)$ is the potential function and $\mathcal{D}$ is the diffusion coefficient. By setting the time-dependent term to zero on the left-hand side of Eq. (32), an exact solution can be readily obtained as

$$p_s(x) = \mathcal{N} \exp[\mathcal{U}(x)/\mathcal{D}], \tag{33}$$

where $p_s(x)$ is the stationary probability density function valid at $t \to \infty$. $\mathcal{N}$ in Eq. (33) is determined from the normalization condition [2]. A double-well potential is the case in which $-\mathcal{U}(x)$ has two minima with a local maximum between in which case the probability density function is bimodal.

B. Stochastic bistable neurodynamical system

A large number of neurons can be approximately described as realizations of a single stochastic dynamics. It is highly desired to describe activities of such neurons statistically based on an ensemble of neurons rather than individually. A single neuron operates by receiving electrochemical signals from other neurons through synapses. When the summation of received signals reaches a critical level, known as the threshold, the neuron sends a signal onto other neurons. The act of sending a signal by the neuron is called neuron firing. The statistical description of the dynamics of neuron firing rates can help us to investigate the dynamics of the neural populations and their interactions [12,13]. This statis-

tical description sometimes is modeled through a multivariate Fokker-Planck equation [14,15].

The temporal dynamics of the firing rates of two different populations of neurons can be described by the following system of stochastic differential equations [3,16]:

$$d\nu_i(t) = \frac{1}{\tau}\left[\phi\left(\lambda_i + \sum_{j=1}^{2} w_{ij}\nu_j(t)\right) - \nu_i(t)\right]dt + \frac{\beta}{\sqrt{\tau}}d\mathcal{W}_i(t), \tag{34}$$

where $\nu_i(t)$ is the population firing rate of population $i=1,2$, w_{ij} is the synaptic strength between populations j and i, and τ is the time constant. λ_i represents the sensory input to the population i and $\phi(\ )$ is the transfer function assumed to be a sigmoid function,

$$\phi(x) = \frac{\nu_{\max}}{1+\exp\left[-\alpha\left(\frac{x}{\nu_c}-1\right)\right]}, \tag{35}$$

where $\nu_{\max}$ is the saturation value and ν_c is the maximal slope. In Eq. (34), $\mathcal{W}_i(t)$ is a Wiener process [2] where $d\mathcal{W}_i(t)=\xi_i(t)\sqrt{dt}$ with $\xi(t)$ denoting a normally distributed random number with mean $\langle\xi_i(t)\rangle=0$ and autocorrelation $\langle\xi_i(t)\xi_j(t')\rangle=\delta_{ij}\delta(t-t')$, where δ_{ij} and $\delta(\ )$ are the Kronecker and Dirac delta functions, respectively. By expanding Eq. (35) through a Taylor series expansion and assuming a bimodal Gaussian distribution [3], differential equations for the first and second moments of the rate of firing from averaging carried out on Eq. (34) are derived. Here, we solve the same problem by the dynamic LSQKD model while treating the sigmoid function in its exact form given by Eq. (35).

Equation (34) represents a system of Langevin equations which is statistically equivalent to the Fokker-Planck equation (1) where $\mathbf{x}\equiv\{\nu_1,\nu_2\}$ and

$$\mathcal{A}_1(\mathbf{x}) \equiv \frac{1}{\tau}[\phi(\lambda_1 + w_{11}\nu_1 + w_{12}\nu_2) - \nu_1], \tag{36}$$

$$\mathcal{A}_2(\mathbf{x}) \equiv \frac{1}{\tau}[\phi(\lambda_2 + w_{21}\nu_1 + w_{22}\nu_2) - \nu_2], \tag{37}$$

$$\mathcal{B}_{11}(\mathbf{x}) = \mathcal{B}_{22}(\mathbf{x}) \equiv \frac{\beta^2}{\tau}, \tag{38}$$

$$\mathcal{B}_{12}(\mathbf{x}) = \mathcal{B}_{21}(\mathbf{x}) = 0. \tag{39}$$

It is noted that $\nu_i(t)$ are the time-dependent random variables governed by the Langevin equation (34), while ν_i are their corresponding independent variables in the phase space.

For the LSQKD formulation of this problem, $\mathbf{D}$ and $\mathbf{E}$ in Eq. (23) are split into two components:

$$\mathbf{D} = \mathbf{D}_1 + \mathbf{D}_2, \tag{40}$$

$$\mathbf{E} = \mathbf{E}_1 + \mathbf{E}_2. \tag{41}$$

In these equations, for the calculation of $\mathbf{D}_1$ and $\mathbf{E}_1$, Eqs. (27) and (28) are used, respectively, where

$$\mathbf{Q} \equiv \mathbf{Q}_1 = (Q_1(g_1) \quad Q_1(g_2))^T, \tag{42}$$

where

$$Q_1(g_k) = \frac{1}{\tau}\frac{\partial}{\partial\nu_1}(\nu_1 g_k) + \frac{1}{\tau}\frac{\partial}{\partial\nu_2}(\nu_2 g_k) - \frac{\beta^2}{2\tau}\left(\frac{\partial^2 g_k}{\partial\nu_1^2} + \frac{\partial^2 g_k}{\partial\nu_2^2}\right). \tag{43}$$

For the calculation of $\mathbf{D}_2$ and $\mathbf{E}_2$ in Eqs. (41) and (40), also Eqs. (27) and (28) are used, respectively, where

$$\mathbf{Q} \equiv \mathbf{Q}_2 = (Q_2(g_1) \quad Q_2(g_2))^T, \tag{44}$$

where

$$Q_2(g_k) = -\frac{1}{\tau}\frac{\partial}{\partial\nu_1}[\phi(\lambda_1 + w_{11}\nu_1 + w_{12}\nu_2)g_k] - \frac{1}{\tau}\frac{\partial}{\partial\nu_2}[\phi(\lambda_2 + w_{21}\nu_1 + w_{22}\nu_2)g_k]. \tag{45}$$

It is noted that $Q_1(g_k)+Q_2(g_k)=Q(g_k)$, where Q is given in Eq. (19). The reason for the split of $\mathbf{D}$ and $\mathbf{E}$, and subsequently of Q, is that $\mathbf{D}_1$ and $\mathbf{E}_1$ can be expressed analytically in terms of $\mathbf{a}$ and $\mathbf{b}$, whereas $\mathbf{D}_2$ and $\mathbf{E}_2$ cannot. Integrals seen in Eqs. (40) and (41) can be evaluated exactly for $\mathbf{D}_1$ and $\mathbf{E}_1$. On the other hand, as seen in Eq. (45), Q_2 depends on ϕ and thus integrals seen in Eqs. (40) and (41) involve ϕ for the calculation of $\mathbf{D}_2$ and $\mathbf{E}_2$. These integrals cannot be evaluated exactly when ϕ is given in the form seen in Eq. (35), so they must be evaluated numerically. In this work, the numerical method of Hermite-Gauss quadrature [17] is employed to evaluate integrations for $\mathbf{D}_2$ and $\mathbf{E}_2$.

Here, we should emphasize that the neurodynamical system presented in this section should not be thought as a double-well potential problem. The reason is that the drift vector $\mathcal{A}\equiv\{\mathcal{A}_1,\mathcal{A}_2\}$ given by Eqs. (36) and (37) cannot be a gradient of a potential function since $\mathcal{A}$ is not curl free, i.e., $\nabla\times\mathcal{A}\neq 0$.

C. Brownian particles in a nonuniform gas

The Brownian motion of particles in a nonuniform gas where there is a gradient of gas velocity can be described by the Fokker-Planck equation [18]. This equation in a one-dimensional fluid flow reads

$$\frac{\partial p}{\partial t} = -\frac{\partial}{\partial x}(up) - \frac{1}{\tau_p}\frac{\partial}{\partial u}\{[v(x,t)-u]p\} + \mathcal{D}\frac{\partial^2 p}{\partial u^2}, \tag{46}$$

where x and u denote the position and velocity of the particle in the phase space, respectively. τ_p is the particle relaxation time constant and $\mathcal{D}$ is the diffusion coefficient. v is the velocity field of the gas, which is a given function of x and t. The thermophoretic effects which are due to the temperature gradient in the gas [18], are assumed to be negligible so their corresponding term is not shown in Eq. (46).

Setting $\mathbf{y}\equiv(x)$, $\mathbf{z}\equiv(u)$, $\mathbf{d}\equiv(\mu,s)$, and $p_1\equiv G$ in Eq. (2), the general formulation given for LSQKD modeling, the PDF is approximated by

$$p(x,u,t) = a(x,t)G(u;\mu(x,t),s(x,t)), \tag{47}$$

where G is a univariate Gaussian function of u where its mean μ and variance s are functions of t as well as x. Substituting for p in Eq. (46) from Eq. (47) results in a residual which can be minimized through the LSQKD approach. This minimization leads to the following set of equations:

$$\frac{\partial a}{\partial t} + \mu\frac{\partial a}{\partial x} + a\frac{\partial \mu}{\partial x} = 0, \tag{48}$$

$$\frac{\partial \mu}{\partial t} + \frac{s}{a}\frac{\partial a}{\partial x} + \mu\frac{\partial \mu}{\partial x} + \frac{1}{4}\frac{\partial s}{\partial x} = \frac{1}{\tau_p}[v(x,t) - \mu], \tag{49}$$

$$\frac{\partial s}{\partial t} + 2s\frac{\partial \mu}{\partial x} + \mu\frac{\partial s}{\partial x} = -\frac{2s}{\tau_p} + 2\mathcal{D}. \tag{50}$$

The important point is that using the LSQKD modeling, we reduce the number of independent variables (x,u,t) in Eq. (46) to (x,t) in the system of equations given above. Also, it is seen that if the last term on the right-hand side of Eq. (50) is set to zero, i.e., no random force acting on the particle, Eqs. (48)–(50) become identical to the equations derived in our previous work [1] in which the evolution of uncertainty in the initial position and velocity of a particle has been studied. It is noted that in that work the formulation has been developed for σ instead of s, where $s=\sigma^2$ denotes the variance in the Gaussian function in Eq. (47).

The particle Fokker-Planck equation (46) is statistically equivalent to

$$\frac{dx(t)}{dt} = u(t), \tag{51}$$

$$\frac{du(t)}{dt} = \frac{1}{\tau_p}[v(x(t),t) - u(t)] + \sqrt{\mathcal{D}}\mathcal{W}(t), \tag{52}$$

where $\mathcal{W}(t)$ is a Wiener process [2], and $x(t)$ and $u(t)$ are the position and velocity of a single Brownian particle in a trajectory (Lagrangian) description. The first term on the right-hand side of Eq. (52) accounts for the drag force acting on the particle from the gas, while the second term is due to the random collisions of gas molecules on the particle.

IV. VERIFICATION METHODOLOGY

In order to conduct the verification of the LSQKD for the Fokker-Planck equations studied in this work, two established methods are employed to compare LSQKD's predictions against. The first method is the MC. The MC, as practiced in its classical form [19], is a very useful and easy-to-implement technique to solve PDEs involving only first-order derivatives, e.g., Fokker-Planck equation (1) at the limit of $\mathcal{B}_{ij}=0$. The Fokker-Planck equation is known as the Liouville equation at this limit for which we have implemented MC in our previous work to verify LSQKD [1]. In the current work we implement MC only for the stochastic bistable neurodynamical system problem at the limit of $\beta=0$. In the next section we detail how the MC is formulated and carried out for this special case.

The stochastic particle method (SPM) is the second method utilized for the verification of LSQKD in Fokker-Planck equations. The SPM is a mesh-free particle method to solve parabolic PDEs through tracking an ensemble of "computational" particles [20–22]. This method, which is sometimes used under different names, has been employed to solve a number of problems ranging from the Vlasov-Fokker-Planck equation [23] encountered in collisional plasmas to the Navier-Stokes equations through vortex-based methods [24]. In particular, referred by the stochastic Lagrangian model, this method is extensively used to solve the Fokker-Planck equations with a high phase-space variable dimension encountered in the PDF modeling of turbulent flows [25–28].

In the SPM, the particles are initially distributed in the phase space using the initial value of the function that the PDE is solved for. In the case of a Fokker-Planck equation, particles are driven in the phase space through the stochastic differential equations (SDEs) statistically equivalent to this equation. For instance, the Fokker-Planck equation governing the stochastic bistable neurodynamical system discussed in Sec. III B, Eq. (34), is solved for $\nu_1(t)$ and $\nu_2(t)$ which show in fact the position of an individual computational particle in the ν_1-ν_2 phase space. At any time such as t the PDF can be constructed from the positions of computational particles distributed in the phase space using

$$p(\mathbf{x},t) = \frac{1}{n_p}\sum_{i=1}^{n_p} H(|\mathbf{x} - \mathbf{x}^{(i)}(t)|), \tag{53}$$

where n_p is the total number of particles, $\mathbf{x}^{(i)}$ denotes the position vector of the ith particle in the phase space, $|\mathbf{r}|$ denotes the magnitude of the vector $\mathbf{r}$, and $H(\,)$ is the kernel function. In this work we use the free-source code of SPLASH developed by [29]. The kernel function used in SPLASH is the cubic spline. It should be noted that depending on the problem physics, e.g., Brownian particle problem discussed in Sec. III C, the computational particles may also represent the real particles.

Here we would like to mention that our choice of the SPM for the verification of the LSQKD is rather due to our more familiarity with the technicalities of this method. Any other method including the method of local characteristic of Warnock and Ellison [30], which directly solves the Fokker-Planck equation, could serve our verification purposes in this study.

V. RESULTS

We first show the results for the double-well potential problem described in Sec. III A. We assume that the potential field in Eq. (32) is

$$\mathcal{U}(x) = -\tfrac{1}{4}(x^2 - 5)^2. \tag{54}$$

By setting $\mathcal{U}'(x)=0$, two stable fixed points are found at $x = \pm\sqrt{5}$ and one unstable point at $x=0$. This is a benchmark problem discussed by Gardiner [2] in detail. Figure 1 shows the results of the stationary probability density function for various values of $\mathcal{D}$ obtained by the exact solution given by

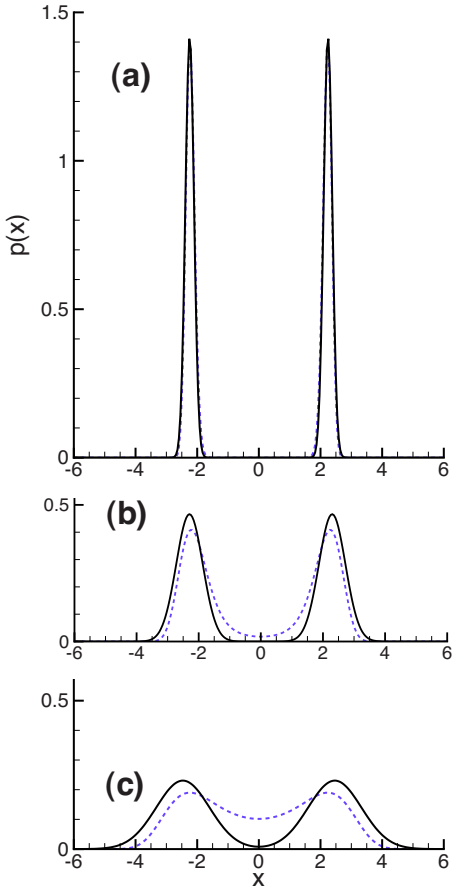

FIG. 1. (Color online) The stationary probability density function for the double-well potential problem by the dynamic LSQKD (solid line) and exact solution (dashed line) shown for three different diffusion coefficients: (a) $\mathcal{D}=0.2$, (b) $\mathcal{D}=2$, and (c) $\mathcal{D}=10$.

Eq. (33) and by the solution obtained by dynamic LSQKD modeling. A very good agreement is seen for the case with $\mathcal{D}=0.2$ in Fig. 1(a). While the deviation between exact and model solutions seems to be acceptable for a higher diffusion $\mathcal{D}=2$, as seen in Fig. 1(b), it is significant for the highest diffusion case $\mathcal{D}=10$ as seen in Fig. 1(c). For the highest diffusion the locations of picks are reasonably well captured by the model, though.

The stochastic bistable neurodynamical system discussed in Sec. III B is studied for these parameters $w_{11}=w_{22}=w_+ - w_I$ and $w_{12}=w_{21}=w_- - w_I$, where $w_I=1.9$, $w_+=2.4$, and $w_- =0.43(w_+ - 1)$ in Eq. (34), and $\alpha=4$ and $\nu_c=\nu_{max}=20$ in Eq. (35). Similar values for these parameters are used by Deco and Martí [3,16].

In order to gain preliminary insight into the stochastic bistable neurodynamical system, we consider it first with no randomness. Figure 2 displays the flow vector field of differential equations,

$$\frac{d\nu_1(t)}{dt} = \frac{\phi[\lambda_1 + w_{11}\nu_1(t) + w_{12}\nu_2(t)] - \nu_1(t)}{\tau}, \tag{55}$$

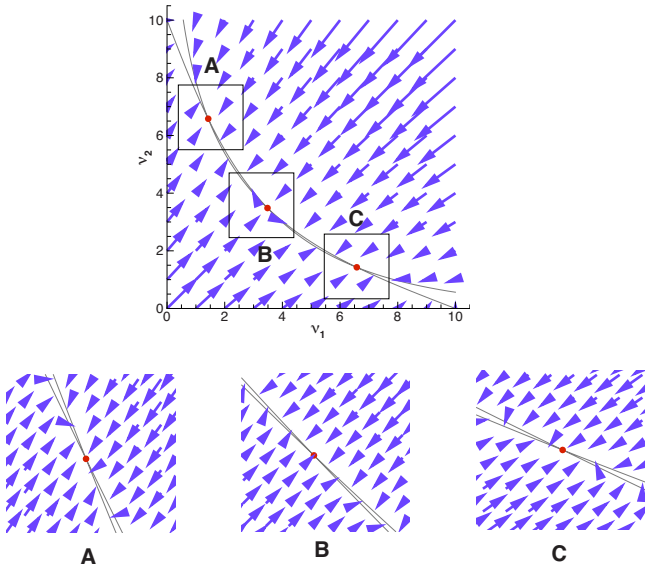

FIG. 2. (Color online) Flow vector field, nullclines, and fixed points (filled circles).

$$\frac{d\nu_2(t)}{dt} = \frac{\phi[\lambda_2 + w_{21}\nu_1(t) + w_{22}\nu_2(t)] - \nu_2(t)}{\tau}, \tag{56}$$

which are the deterministic version of SDEs given by Eq. (34) where $\beta=0$. Nullclines associated with $d\nu_1(t)/dt=0$ and $d\nu_2(t)/dt=0$, which have the equations $\phi(\lambda_1+w_{11}\nu_1 + w_{12}\nu_2)-\nu_1=0$ and $\phi(\lambda_2+w_{21}\nu_1+w_{22}\nu_2)-\nu_2=0$, respectively, are seen in Fig. 2. The filled circles in this figure show the location of the fixed points where nullclines intersect. The middle fixed point is unstable, whereas the two others are stable. Two nullclines in the midsection—starting from one stable fixed point, passing through the unstable fixed point, and ending to the other stable fixed point—are very close to each other. This means that the magnitude of vector field is very small in a narrow region along the nullclines compared to the rest of the region.

In order to assess the accuracy of the LSQKD method in the neurodynamical system at the limit of no randomness, its results are compared against the results obtained by the method of characteristics (MC). Here, we describe how the MC is formulated for this problem. Having set the diffusion term in Eq. (1) to zero and substituted Eqs. (36) and (37) in Eq. (1), the equation is rearranged in the following form:

$$\begin{aligned}\frac{\partial p}{\partial t} &+ \frac{1}{\tau}[\phi(\lambda_1 + w_{11}\nu_1 + w_{12}\nu_2) - \nu_1]\frac{\partial p}{\partial \nu_1} \\ &+ \frac{1}{\tau}[\phi(\lambda_2 + w_{21}\nu_1 + w_{22}\nu_2) - \nu_2]\frac{\partial p}{\partial \nu_2} \\ &= \frac{p}{\tau}[2 - w_{11}\phi'(\lambda_1 + w_{11}\nu_1 + w_{12}\nu_2) \\ &- w_{22}\phi'(\lambda_2 + w_{21}\nu_1 + w_{22}\nu_2)],\end{aligned} \tag{57}$$

where $\phi' = d\phi(x)/dx$. Equation (57) in the trajectory description reads

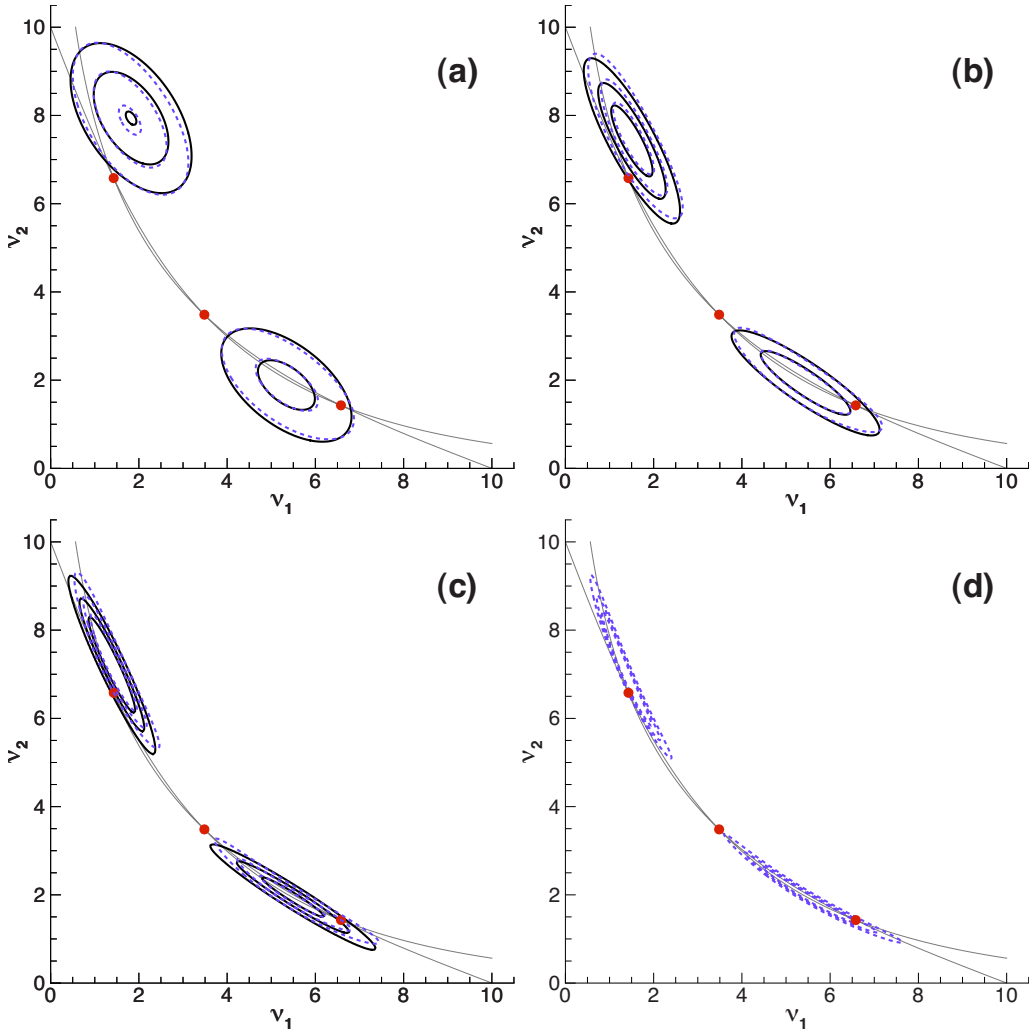

FIG. 3. (Color online) Contours of the probability density function $p(\nu_1,\nu_2,t)$ for the bistable stochastic neurodynamical system obtained by the dynamic LSQKD (solid line) and the method of characteristics (dashed line) for $\beta=0$ at (a) $t=0.005$, (b) $t=0.01$, (c) $t=0.015$, and (d) $t=0.02$. Contour values are 0.01, 0.1, and 0.4 from the outermost to the innermost contour, respectively.

$$\frac{dz(t)}{dt} = \frac{z(t)}{\tau}\{2 - w_{11}\phi'[\lambda_1 + w_{11}\nu_1(t) + w_{12}\nu_2(t)] - w_{22}\phi'[\lambda_2 + w_{21}\nu_1(t) + w_{22}\nu_2(t)]\}. \quad (58)$$

In the MC method, this equation is solved along with Eqs. (55) and (56) in time employing the initial condition $z(0)=p_0(\nu_1(0),\nu_2(0))$, where p_0 is the initial condition for p, i.e., $p_0(\nu_1,\nu_2)=p(\nu_1,\nu_2,0)$. Then the value of p at the position $\nu_1=\nu_1(t)$ and $\nu_2=\nu_2(t)$, and time t is the same as the value of z at time t. That means $p(\nu_1(t),\nu_2(t),t)=z(t)$.

With the initial condition set to

$$\mathbf{a} = (0.3 \quad 0.7)^T,$$

$$\mathbf{b} = (5.2 \quad 1.8 \quad 0.5 \quad 0.5 \quad 0 \quad 2.3 \quad 8.7 \quad 0.5 \quad 0.5 \quad 0)^T, \quad (59)$$

we perform LSQKD and MC simulations for $\beta=0$ which corresponds to a nonrandom case. The contours of p on the ν_1-ν_2 plane are displayed in Fig. 3 for various times. Good agreements between LSQKD and MC are seen in Figs. 3(a)–3(c). We observe that the contours of LSQKD are ellipses that with the increase in time from Figs. 3(a)–3(c) their major axes align with the nullclines while their minor axes become smaller. Smaller minor axes correspond to a smaller determinant of the coefficient matrix on the left-hand side of Eq. (23). Therefore, the inversion of the coefficient matrix eventually becomes impossible after a certain time as the minor axes of contour ellipses further shrink. This is when the simulation by LSQKD is terminated and that is the reason for not having a LSKQD result in Fig. 3(d), which is for the largest time seen in this figure. As time progresses the contours of p further shrink along the major axes as well. Theoretically, at the limit $t\to\infty$ all contours should become points on two stable fixed points or better say that p should become bimodal with two delta functions at the stable fixed points. We observe this with the continuation of MC simulations.

The LSQKD is verified for the bistable neurodynamical system for $\beta\neq 0$ comparing its results against the results obtained by SPM illustrated in Sec. IV. Figure 4 shows the

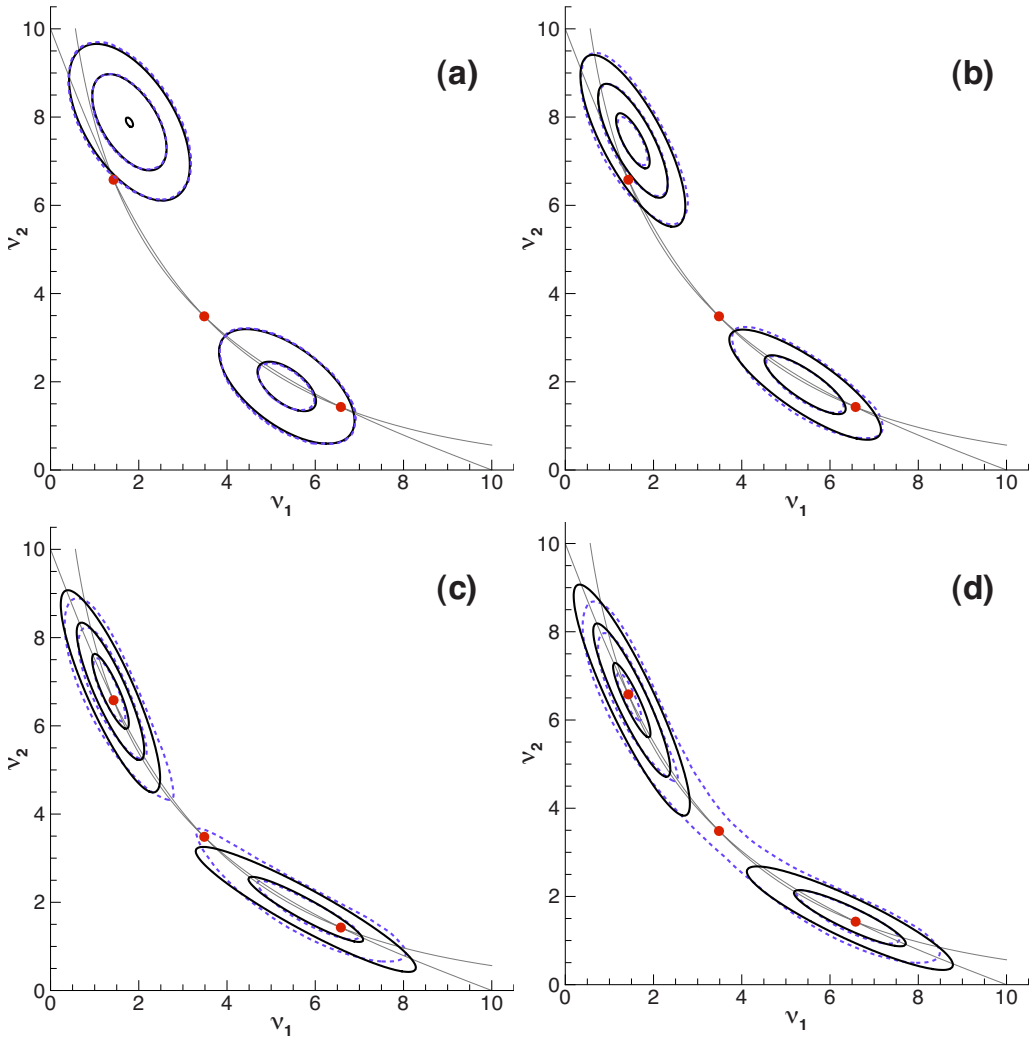

FIG. 4. (Color online) Contours of the probability density function $p(\nu_1,\nu_2,t)$ for the stochastic bistable neurodynamical system obtained by the dynamic LSQKD (solid line) and SPM (dashed line) for β=0.3 at (a) t=0.005, (b) t=0.01, (c) t=0.1, and (d) t=2. Contour values are 0.01, 0.1, and 0.4 from the outermost to the innermost contour, respectively.

contours of p obtained by LSQKD and SPM for β=0.3 at four different times. For the LSQKD case, the initial conditions are set to Eq. (59) where **a** and **b** are defined by Eqs. (14) and (15), respectively. Corresponding to the initial values of **a** given by Eq. (59), where a_1=0.3 and a_2=0.7, the SPM simulations are conducted with 30% of computational particles released with g_1 distribution while 70% released with g_2 distribution. g_1 and g_2 are Gaussian given by Eq. (10) where $\mu_{1,1}$=5.2, $\mu_{2,1}$=1.8, $\mu_{1,2}$=2.3, $\mu_{2,2}$=8.7, $\sigma_{1,1}$ =$\sigma_{2,1}$=$\sigma_{1,2}$=$\sigma_{2,2}$=0.5, and c_1=c_2=0. A very good agreement between LSQKD and SPM results is observed at first two times shown in Figs. 4(a) and 4(b), respectively. Moreover, the agreement between LSQKD and SPM seen in Figs. 4(c) and 4(d), which are for later times, is reasonably good. The diffusion effects in Fig. 4 can be observed via comparing it to Fig. 3, which is for the nondiffusive case β=0 at corresponding times. Comparing Fig. 3(a) to Fig. 4(a), which both are at t=0.005, and Fig. 4(b) to Fig. 3(b), which both are at t=0.01, reveals that the drift effects at early times are more significant than the diffusion effects. In other words, the drift mechanism is predominant at the early stage of the evolution of p. Later on an equilibrium is reached between drift and diffusion in the direction transverse to nullclines. The sizes of minor axes of elliptical contours remain almost unchanged from Fig. 4(c) to Fig. 4(d).

The stationary state of the stochastic neurodynamical system studied in this work is displayed in Fig. 5 for β=0.2, 0.3, and 0.4. At the stationary state the drift and diffusion effects are in equilibrium in both lateral and transversal directions to the nullclines. In addition there is a balance between two neural populations represented by two modes of p. This balance is due to "escaping particles" [2], presented by a low p contour value of 0.01 for the SPM case around the unstable fixed point in the middle, from one neural population to another. Practically, because of these escaping particles, the population balance is reached between two populations corresponding to two stable states in the system. There is a fairly good match between SPM and LSQKD p contours in Figs. 5(a) and 5(b) presenting β=0.2 and 0.3, respectively. On the other hand, LSQKD fails to represent the bimodal probability density for β=0.4 as seen in Fig. 5(c). In this case, two Gaussian functions are close to each other both

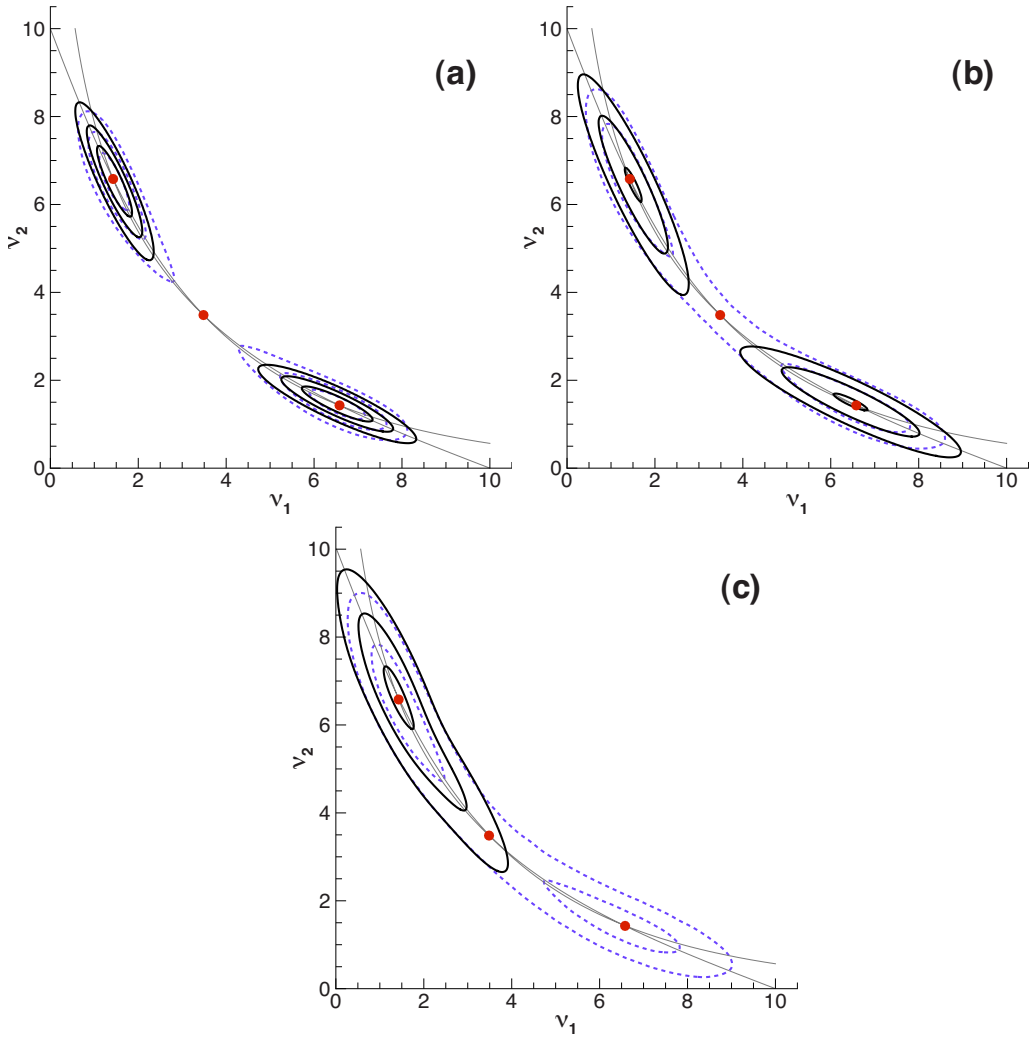

FIG. 5. (Color online) Contours of stationary probability density function $p(\nu_1,\nu_2,\infty)$ for the stochastic bistable neurodynamical system obtained by the dynamic LSQKD (solid line) and SPM (dashed line) for (a) β=0.2, (b) β=0.3, and (c) β=0.4. Contours are for 0.01, 0.1, and 0.4 from the outermost to the innermost contour, respectively.

representing one mode of the PDF. The broken contour ellipses of LSQKD are due to these two Gaussian functions with centers next to each other on the nullclines and on one side of the unstable fixed point.

In this section from here on out we discuss the case and results obtained for Brownian particles in a nonuniform gas described in Sec. III C. The velocity of the gas $v(x,t)$ required in Eqs. (46) and (49) is assumed to vary in space according to

$$v(x,t) = 1 + v_0 \sin(2\pi x), \tag{60}$$

where v_0 is a constant. The reason for having assumed such a function for the variation of the fluid velocity is that the sinusoidal function results in a multimodal behavior of the PDF in the x direction [1]. To initiate the simulations for the Brownian particles, it is assumed that the PDF is initially bivariate Gaussian,

$$p(x,u,0) = \frac{1}{2\pi|\mathbf{\Sigma}|^{1/2}}\exp\left(-\frac{1}{2}\mathbf{x}^T\mathbf{\Sigma}^{-1}\mathbf{x}\right), \tag{61}$$

where

$$\mathbf{x} = \begin{pmatrix} x \\ u \end{pmatrix}, \quad \mathbf{\Sigma} = \begin{pmatrix} 0.05 & 0 \\ 0 & 0.05 \end{pmatrix}. \tag{62}$$

The LSQKD and SPM are conducted with this initial PDF for parameters τ_p=1 in Eq. (46) and v_0=0.3 in Eq. (60). The system of equations (48)–(50), equations derived by LSQKD modeling, is discretized in the x direction through finite difference upwind scheme and solved in time numerically through the explicit Euler scheme [31,32].

Figure 6 displays the PDF contours of Brownian particles at three different time levels of t=1, 2, and 3. PDF contours at t=0 (not shown in the figure) are circles with centers at x=0 and u=0 corresponding to the initial Gaussian PDF given in Eq. (61). Although the PDF greatly deviates from the initial Gaussian function as time increases, this deviation is attributed to the fact that different particles at different locations on the phase space experience different drag forces according to Eq. (52). The multimodality of PDF in the x direction is evidently seen in Fig. 6(c), while the PDF is unimodal in the u direction. An excellent performance by the

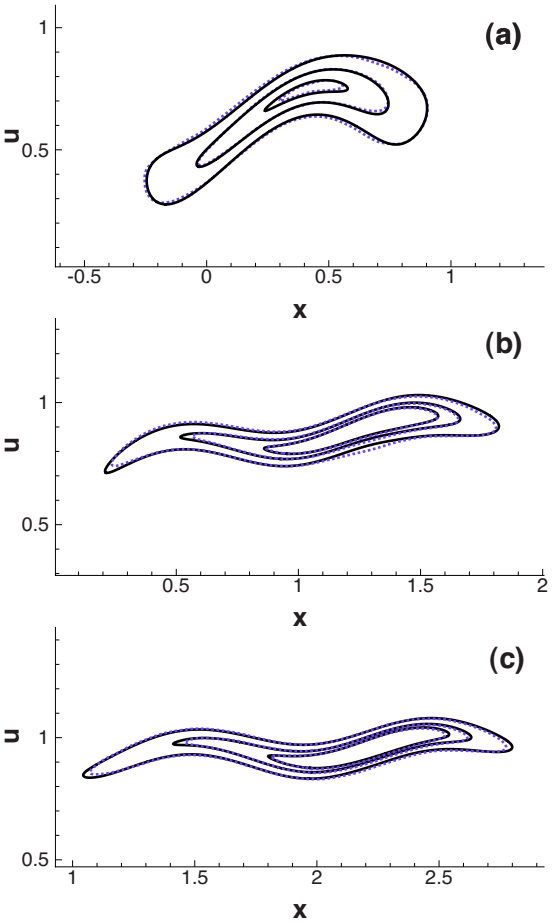

FIG. 6. (Color online) Contours of probability density function $p(x,u,t)$ for Brownian particles in a nonuniform gas for $\mathcal{D}=0.001$ obtained by dynamic LSQKD (solid line) and SPM (dashed line) at (a) $t=1$, (b) $t=2$, and (c) $t=3$. Contours are for $p(x,u,t)=1$, 4, and 7 from the outermost to the innermost contour, respectively.

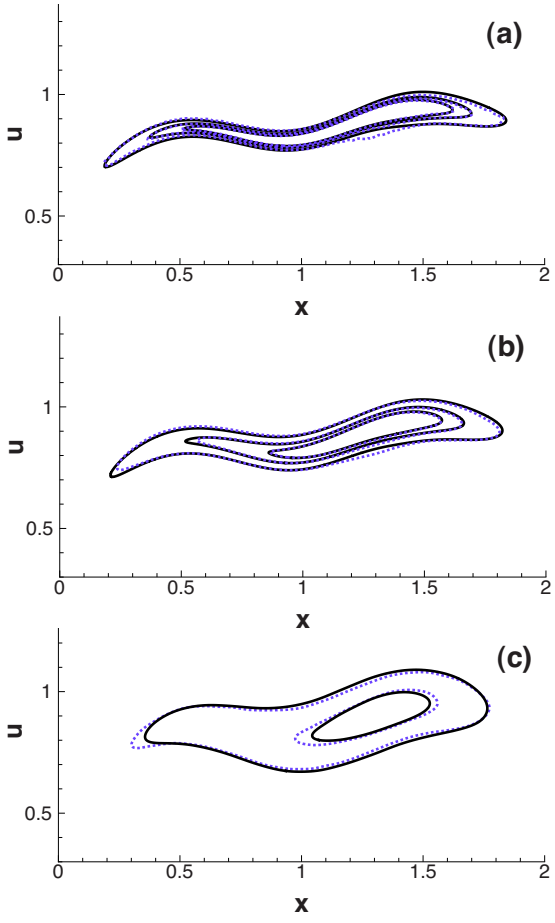

FIG. 7. (Color online) Contours of probability density function $p(x,u,t)$ for Brownian particles in a nonuniform gas at $t=2$ obtained by dynamic LSQKD (solid line) and SPM (dashed line) for (a) $\mathcal{D}=1\times10^{-4}$, (b) $\mathcal{D}=1\times10^{-3}$, and (c) $\mathcal{D}=1\times10^{-2}$. Contours are for $p(x,u,t)=1$, 4, and 7 in (a) and (b), and $p(x,u,t)=1$ and 4 in (c) from the outermost to the innermost contour, respectively.

LSQDK is observed as its PDF contours and their SPM counterparts are very close to each other.

Figure 7 shows the PDF contours of Brownian particles for three different $\mathcal{D}=1\times10^{-4}$, 1×10^{-3}, and 1×10^{-2} at the same $t=2$. It is seen that with the increase in $\mathcal{D}$ the width of contours increases in the u direction. This increase is expected and it is due to the effect of random forces applied on particles as modeled by the second term on the right-hand side of Eq. (52). A very good agreement is seen between LSQKD and PDF in Figs. 7(a) and 7(b). This agreement is good in Fig. 7(c) which corresponds to the case with the largest $\mathcal{D}$.

VI. DISCUSSION AND CONCLUSIONS

Three sample problems are studied in this work where their corresponding Fokker-Planck equation is modeled by the dynamic LSQKD and the results are verified against the results obtained by the MC or the SPM. The first one is a double-well potential problem with one phase-space variable in its Fokker-Planck equation and the second one is a stochastic bistable neurodynamical system with two phase-space variables in its Fokker-Planck equation. In both problems through LSQKD modeling, a system of ordinary differential equations (ODEs) is derived. Our results obtained for the double-well potential problem and the stochastic neurodynamical system reveal that the LSQKD is a good approximation for these cases with low to medium diffusivity. For high diffusive cases, the LSQKD either fails to represent the bimodal shape of the PDF or poorly approximates the PDF. The third problem studied in this work is the motion of Brownian particles in a nonuniform gas for which the corresponding Fokker-Planck equation with two phase-space variables is modeled through LSQKD modeling by which a system of three PDEs with only one phase-space variable is derived. For a wide range of diffusion coefficients, a very good performance by the LSQKD is observed for this problem.

One way to improve the accuracy of LSQKD for the bistable neurodynamical system especially in the case of high diffusivity would be to approximate the PDF with a larger number of Gaussian functions used to construct the kernel density function. In this case the higher accuracy would be achieved with a price to pay; that is, to deal with a

system of ODEs with a large number of unknowns. We think that the dynamic LSQKD model with two Gaussian functions should be thought as a good starting point to conduct a preliminarily analysis of the Fokker-Planck equations for which a bimodal PDF is expected. It is definitely much safer to use it for low diffusive cases.

The dynamic LSQKD is an efficient model for solving the PDF governed by the Fokker-Planck equation as instead of solving this partial differential equation, directly, one solves a system of ordinary equations with time as the independent variable or solves a system of PDEs with time and a reduced number of phase-space variables as independent variables. Due to the gained dimension reduction through the LSQKD modeling, it is computationally less expensive. For instance, the LSQKD models the Fokker-Planck equation (46) given in the x-u space for the case of Brownian particles in a nonuniform gas through Eqs. (48)–(50) in the x space. In this example the LSQKD approximates the variation of the PDF by a Gaussian function in the u direction, as seen in Eq. (47); therefore, the numerical discretization with sufficient resolution (sufficient number of particles) needs to be carried out only in the x direction for Eqs. (48)–(50). Consequently, the LSQKD is computationally much less expensive than the SPM for which the numerical discretization with sufficient resolution must be carried out in both x and u directions. In other words, the SPM directly solves the Fokker-Planck equation in two dimensions, while the LSQKD indirectly solves it through three coupled model equations in one dimension. The CPU time for a typical run in the case of Brownian particles in a nonuniform gas is 1735 s by the SPM with 4×10^5 particles, while for the same setup it is 170 s by the LSQKD with 1.6×10^4 one-dimensional grid points. All computations are performed on a Mac OS X with a 2.4 GHz Intel Core 2 Duo CPU and a 4 GB 1067 MHz DDR3 memory. It is noted that this supremacy of the LSQKD in the computational efficiency is gained having assumed that the PDF is Gaussian in the u direction. Obviously for problems with strong non-Gaussianity, a univariate Gaussian assumption is not a good approximation. Employing multiple Gaussian functions, i.e., increasing K in Eq. (2), or employing basis functions other than the Gaussian function which have more parameters may improve the approximation while it increases the computational costs.

[1] C. Pantano and B. Shotorban, Phys. Rev. E **76**, 066705 (2007).
[2] C. W. Gardiner, *Handbook of Stochastic Methods* (Springer-Verlag, New York, 2004).
[3] G. Deco and D. Martí, Phys. Rev. E **75**, 031913 (2007).
[4] Y. B. Gaididei, C. Gorria, P. L. Christiansen, and M. P. S. Sørensen, Phys. Rev. E **78**, 051908 (2008).
[5] R. Vezzoli, C. De Michele, H. Pavlopoulos, and R. J. Scholes, Phys. Rev. E **77**, 051908 (2008).
[6] R. Benzi and D. R. Nelson, Physica D **238**, 2003 (2009).
[7] E. Fix and J. L. Hodges, USAF School of Aviation Medicine Technical Report No. 21-49-004, 1951 (unpublished).
[8] B. W. Silverman, *Density Estimation for Statistics and Data Analysis* (Chapman & Hall/CRC, London, 1986).
[9] B. W. Silverman and M. C. Jones, Int. Statist. Rev. **57**, 233 (1989).
[10] D. W. Scott, *Multivariate Density Estimation: Theory, Practice, and Visualization* (Wiley, New York, 1992).
[11] L. C. Charles and R. J. Hanson, *Solving Least Squares Problems* (Society for Industrial and Applied Mathematics, Philadelphia, 1995).
[12] H. C. Tuckwell, *Introduction to Theoretical Neurobiology* (Cambridge University Press, Cambridge, England, 1988).
[13] A. Renart, N. Brunel, and X. Wang, in *Computational Neuroscience: A Comprehensive Approach*, edited by J. Feng (Chapman and Hall, Boca Raton, FL, 2003), pp. 431–490.
[14] N. Brunel and V. Hakim, Neural Comput. **11**, 1621 (1999).
[15] H. Câteau and A. D. Reyes, Phys. Rev. Lett. **96**, 058101 (2006).
[16] G. Deco and D. Martí, Biol. Cybern. **96**, 487 (2007).
[17] F. B. Hildebrand, *Introduction to Numerical Analysis*, 2nd ed. (Dover Publications, New York, 1987).
[18] J. Fernandez de la Mora and J. M. Mercer, Phys. Rev. A **26**, 2178 (1982).
[19] S. J. Farlow, *Partial Differential Equations for Scientists and Engineers* (Courier Dover Publications, Mineola, NY, 1993).
[20] D. Talay, *Probabilistic Models for Nonlinear Partial Differential Equations*, edited by D. Talay and L. Tubaro (Springer, Berlin, 1996), pp. 148–196.
[21] D. Stanescu, D. Kim, and W. A. Woyczynski, J. Comput. Phys. **206**, 706 (2005).
[22] M. Bossy, *GRIP—Research Group on Particle Interactions*, ESAIM Proceedings Vol. 15 (EDP Sciences, Les Ulis, 2005), pp. 18–57.
[23] K. J. Havlak and H. D. Victory, SIAM (Soc. Ind. Appl. Math.) J. Numer. Anal. **33**, 291 (1996).
[24] A. J. Chorin, J. Fluid Mech. **57**, 785 (1973).
[25] S. B. Pope, Pror. Energy Combust. Sci. **11**, 119 (1985).
[26] S. B. Pope, Annu. Rev. Fluid Mech. **26**, 23 (1994).
[27] S. B. Pope, *Turbulent Flows* (Cambridge University Press, Cambridge, UK, 2000).
[28] J.-P. Minier and E. Peirano, Phys. Rep. **352**, 1 (2001).
[29] D. J. Price, Publ. - Astron. Soc. Aust. **24**, 159 (2007).
[30] R. Warnock and J. Ellison, *The Physics of High Brightness Beams*:Proceedings of the 2nd ICFA Advanced Accelerator Workshop, edited by J. Rosenzweig and L. Serafini (World Scientific, Singapore, 2000).
[31] C. A. J. Fletcher, *Computational Techniques for Fluid Dynamics* (Springer-Verlag, Berlin, 1988), Vol. I.
[32] C. A. J. Fletcher, *Computational Techniques for Fluid Dynamics* (Springer-Verlag, Berlin, 1988), Vol. II.